

LETTER • OPEN ACCESS

# Restoration of weak localization in bilayer graphene by a molecular thin film

To cite this article: Anise Mansour *et al* 2026 *2D Mater.* **13** 021001

View the [article online](#) for updates and enhancements.

## You may also like

- [Atomic-scale thermoelectric imaging of sublattice symmetry in epitaxial bilayer graphene](#)  
Sanghee Cho, Seungil Baek, Jaeuk Seo et al.
- [Field-resilient supercurrent rectification in NbSe<sub>2</sub> van der Waals Josephson junction](#)  
Annu Anns Sunny, Parvathy Gireesan and Madhu Thalakulam
- [Strain-tunable magnetic correlations in spin liquid candidate Nb<sub>3</sub>Cl<sub>7</sub>](#)  
Tharindu Fernando and Ting Cao



## LETTER

## OPEN ACCESS

RECEIVED  
15 September 2025REVISED  
2 February 2026ACCEPTED FOR PUBLICATION  
9 February 2026PUBLISHED  
25 February 2026

Original content from this work may be used under the terms of the [Creative Commons Attribution 4.0 licence](https://creativecommons.org/licenses/by/4.0/).

Any further distribution of this work must maintain attribution to the author(s) and the title of the work, journal citation and DOI.



# Restoration of weak localization in bilayer graphene by a molecular thin film

Anise Mansour<sup>1,6</sup> , Deanna Diaz<sup>1,6</sup>, Movindu K D Dissanayake Mudiyansele<sup>1,6</sup>, Erin Henkhaus<sup>1</sup>, Jungyoun Cho<sup>2</sup>, Vinh Tran<sup>1</sup>, Francisco Ramirez<sup>1</sup>, Eric Corona-Oceguera<sup>1</sup>, Joshua Luna<sup>1</sup>, Kenta Kodama<sup>1</sup>, Yueyun Chen<sup>2,3</sup>, Ho Chan<sup>2,3</sup>, Jacob Weber<sup>1</sup>, Blake Koford<sup>1</sup>, Patrick Barfield<sup>1</sup>, Maya Martinez<sup>1</sup>, Kenji Watanabe<sup>4</sup> , Takashi Taniguchi<sup>5</sup>, B C Regan<sup>2,3</sup>, Matthew Mecklenburg<sup>2</sup>, Sarah Grefe<sup>1</sup>, Thomas Gredig<sup>1</sup> and Claudia Ojeda-Aristizabal<sup>1,\*</sup>

<sup>1</sup> Department of Physics and Astronomy, California State University Long Beach, Long Beach, CA 90840, United States of America

<sup>2</sup> California NanoSystems Institute (CNSI), University of California, Los Angeles, CA 90095, United States of America

<sup>3</sup> Department of Physics and Astronomy, University of California, Los Angeles, CA 90095, United States of America

<sup>4</sup> Research Center for Electronic and Optical Materials, National Institute for Materials Science, 1-1 Namiki, Tsukuba 305-0044, Japan

<sup>5</sup> Research Center for Materials Nanoarchitectonics, National Institute for Materials Science, 1-1 Namiki, Tsukuba 305-0044, Japan

<sup>6</sup> AM, DD and MKDDM contributed equally to this work.

\* Author to whom any correspondence should be addressed.

E-mail: [Claudia.Ojeda-Aristizabal@csulb.edu](mailto:Claudia.Ojeda-Aristizabal@csulb.edu)

**Keywords:** weak localization, bilayer graphene, phthalocyanines

Supplementary material for this article is available [online](#)

## Abstract

Quantum coherent effects can be probed in multilayer graphene through electronic transport measurements at low temperatures. In particular, bilayer graphene (BLG) is known to be susceptible to quantum interference corrections of the conductivity, presenting weak localization at all electronic densities, and dependent on different scattering mechanisms such as those related to the trigonal warping of the electron dispersion near the K and K' valleys. Proximity effects with a molecular thin film influence these scattering mechanisms, which can be quantified through the known theory of magnetoconductance for BLG. Here, we present electronic transport measurements in a copper-phthalocyanine (CuPc) / BLG / hexagonal boron nitride (h-BN) heterostructure that suggest the restoration of weak localization in BLG, associated to a reduction of trigonal warping effects, that are known to suppress weak localization in BLG. Additionally, we observe a charge transfer of  $3.6 \times 10^{12} \text{ cm}^{-2}$  from the BLG to the molecules, as well as a very small degradation of the mobility of the BLG/h-BN heterostructure upon the deposition of CuPc. The molecular arrangement of the CuPc thin film is characterized in a control sample through transmission electron microscopy, that we relate to the electronic transport results.

## 1. Introduction

In the mesoscopic regime, that is, when the dimensions of a system are small enough to be sensitive to quantum effects and large enough to take into account the contribution of multiple electrons, the quantum interference of electronic trajectories leads to a correction of the conductance that is intimately linked to the character of the charge carriers. In general, such correction survives even after averaging over disorder, and may appear in more macroscopic samples. In graphene, carriers are chiral, their pseudo-spin, related to the existence of two

atoms per unit cell, is either parallel or anti-parallel to the momentum. This makes that if an electron in graphene completes a closed trajectory, the electron wavefunction will acquire an additional phase of  $\pi$ , leading to a destructive interference of the electronic wavefunctions when the electrons propagate in opposite directions around a trajectory [1]. In contrast, the carriers' wave function in bilayer graphene (BLG) while also being chiral, have a geometric phase of  $2\pi$  leading instead to a constructive interference for similar interfering electronic trajectories. This phenomenon in a BLG sample increases the probability of electrons returning to the origin, that in the frame

of quantum diffusion, is related to the interference of pair of trajectories that follow a train of identical collisions, but in opposite directions, forming a loop. The contribution of these trajectories to the conductance decreases the probability of reaching the drain electrode of the sample, resulting in a decrease of electrical conductance with respect to its classical value in the frame of the Drude model [2]. This effect is known as weak localization and can be detected by applying a small magnetic field perpendicular to the sample, that adds an additional phase to the interfering electronic wavefunctions and destroys the interference, resulting in a positive magnetoconductance. In BLG, weak localization is different from the one present in conventional 2-dimensional systems in that it is sensitive not only to inelastic processes that break the phase coherence but also, to elastic scattering events such as intervalley scattering, associated to sharp defects that are able to scatter electrons between the two valleys of BLG. Furthermore, weak localization in BLG is affected by the trigonal warping of the energy spectrum of the carriers, as well as other intravalley scattering rates [2, 3].

The presence of a molecular thin film is able to influence these quantum interference effects. Previous works on monolayer graphene covered with Pt-porphyrines have found that the magnetic moment of these molecules, tunable with the vertical electric field imposed by a gate voltage, has a profound impact on quantum coherent phenomena in graphene, such as universal conductance fluctuations and superconducting proximity effects [4]. Time reversal symmetry breaking brought by the magnetic moment in these molecules creates an odd component in the conductance fluctuations as well as a suppression of the supercurrent in superconductor/graphene/superconductor junctions. Other works on graphene decorated with adatoms have also found signature of modified quantum interference effects, that points to a decrease in weak localization due to the presence of the adatoms and an increase of intervalley scattering, despite the expected stronger long-range intravalley Coulomb scattering from the adatoms. It has also been shown that the presence of the adatoms significantly deteriorates the electronic mobility of the original device [5, 6].

Here, we study the electronic transport of a copper-phthalocyanine (CuPc)/BLG/hexagonal boron nitride (h-BN) heterostructure in the mesoscopic regime. Phthalocyanines are macrocyclic planar aromatic molecules that admit at their center any transition metal from the periodic table, making them highly versatile molecules (see figure 1). CuPc is the most studied phthalocyanine, with a copper ion that has an unpaired electron spin, making it a paramagnetic metal-organic molecule of spin angular momentum  $s = 1/2$  [7]. In the bulk, the

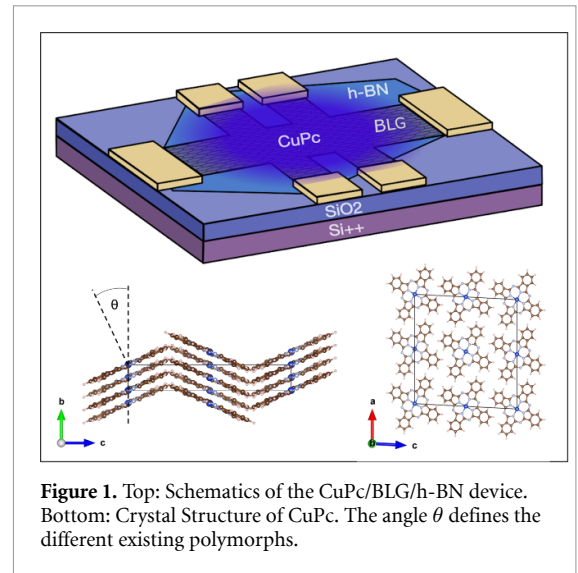


**Figure 1.** Top: Schematics of the CuPc/BLG/h-BN device. Bottom: Crystal Structure of CuPc. The angle  $\theta$  defines the different existing polymorphs.

copper atoms of CuPc have tendency to form one-dimensional chains along the b-axis, as a result of van der Waals molecule-molecule interactions being stronger when the molecules are face-to-face rather than side-to-side. There are different polymorphs of CuPc, distinguished by the angle  $\theta$  between the b-axis and the normal to the plane of the molecule. In the form of a thin film, CuPc grows in a lying configuration for most metallic substrates. When deposited at room temperature, CuPc tends to form a metastable phase known as the  $\alpha$  phase, where  $\theta \approx 25^\circ$  (see figure 1) [7].

Our measurements suggest that the presence of CuPc has the effect of restoring weak localization on the BLG/h-BN heterostructure. In contrast to our work, BLG when in proximity to transition metal dichalcogenides, completely destroys weak localization and leads to weak antilocalization at certain electronic densities, as reported in [8, 9], as a result of proximity-induced Spin-orbit coupling (SOC). SOC in materials such as WSe<sub>2</sub> can be as large as 0.5 eV [10] compared to a few meV in CuPc. [11]. In our work, the molecules do not change Berry phase from  $2\pi$  to  $\pi$ , as is the case when SOC is induced. Instead, they attenuate scattering events that have a tendency to add an additional phase difference to the interfering electronic wave functions that lead to weak localization. The attenuation of these scattering events reinforces the interference effects, manifested as a stronger weak localization dip in the magnetoconductance, in the presence of the molecules.

A fit to the theory for weak localization in BLG allows us to identify a longer intravalley scattering time when the CuPc molecules are deposited. In BLG, this characteristic time is associated mostly to trigonal warping, and a negligible contribution from intravalley Cooperon modes, as detailed in [12]. Our

measurements show a restoration of weak localization in BLG upon deposition of the CuPc molecules and suggest a possible reduction of the trigonal warping in BLG. Additionally, we observe an important charge transfer from the BLG to the CuPc molecules and a reasonable preservation of the mobility of the BLG/h-BN heterostructure upon the deposition of the molecules.

## 2. Sample fabrication

A heterostructure of BLG/h-BN was fabricated using the method introduced in [13], and detailed in the supplemental material [14]. The sample was characterized through Raman spectroscopy. By measuring the intensity ratio of the 2D and G peaks, we identified our sample as BLG. (See in supplemental material [14] Raman data (figure S1), including [15–17]).

The BLG was coated with PMMA 495 and PMMA 950 in order to define electrode patterns through electron beam lithography. Titanium and gold (10 nm/40 nm) were later deposited via electron beam evaporation.

Transport measurements were conducted on the device prior to the deposition of CuPc, as will be detailed later. The CuPc was thermally evaporated using a commercially available high purity powder of CuPc (Ted Pella) using an organic materials- dedicated thermal evaporator. The deposition was performed at  $0.3 \text{ \AA s}^{-1}$  until reaching a thickness of 22 nm in a base pressure of  $1 \times 10^{-6}$  Torr. The sample was kept at room temperature during the deposition process. Simultaneously, CuPc was deposited on a control sample, made of suspended graphene on lacey carbon, compatible with transmission electron microscopy (TEM) experiments.

## 3. Sample characterization through 4D scanning TEM(STEM)

TEM is an imaging technique that utilizes high-energy electrons to probe thin samples, generating images based on the electron-sample interactions. Unlike conventional TEM, which uses a broad electron beam, STEM employs a finely focused electron probe. This reduction in spot size results in increased electron fluence, allowing for high-resolution imaging and diffraction data acquisition at specific sample locations. 4D-STEM measures the 2D diffraction pattern at each position of a 2D STEM map, creating a 4D data set. We chose this diffraction space imaging over real-space imaging as it enables higher resolution for a given electron dose, minimizing radiation damage to beam-sensitive samples such as phthalocyanine molecules. 4D-STEM allowed us to resolve individual CuPc crystals in our control TEM-compatible sample of CuPc/ suspended graphene.

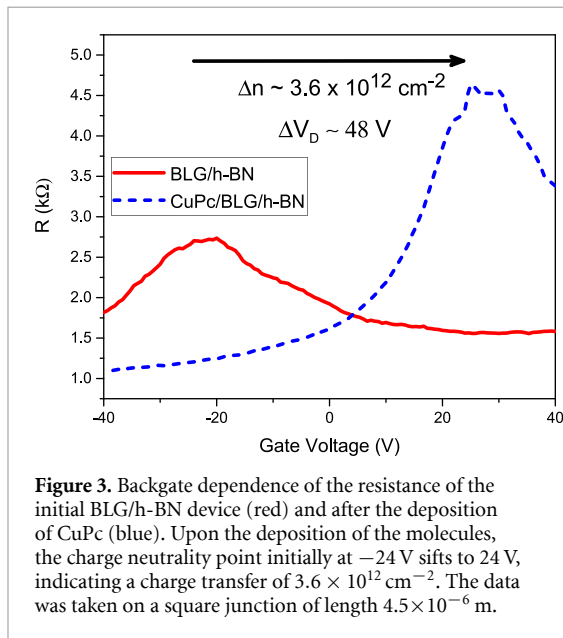
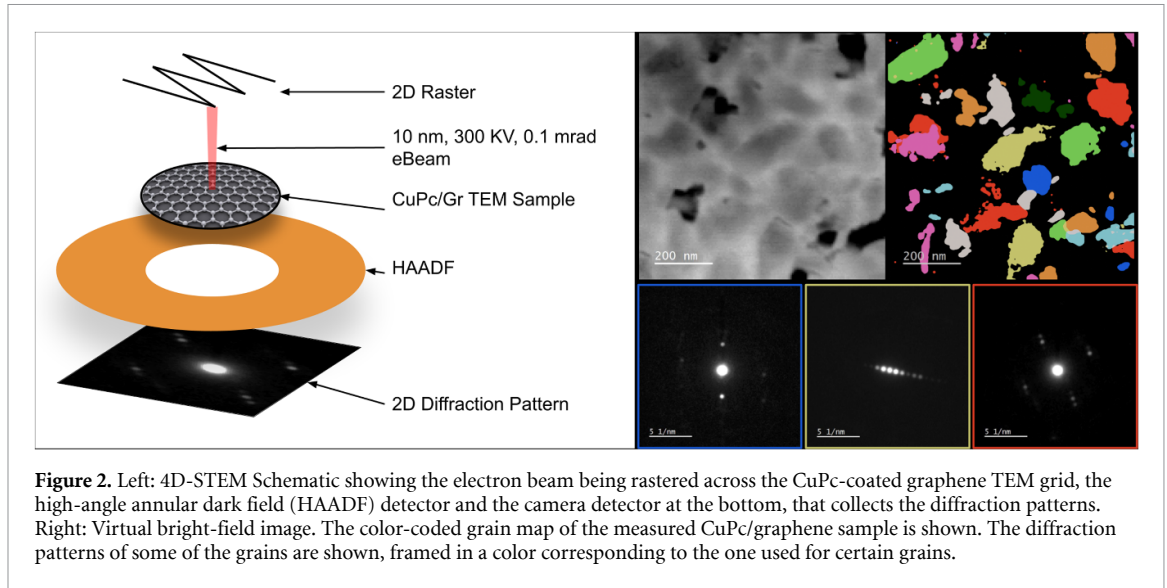
Figure 2 illustrates the 4D-STEM measurement, performed at the BioPACIFIC MIP user facilities at

UCLA. A small electron beam is rastered across a CuPc-coated graphene TEM grid. Live 2D spatial images are first captured using the high-angle annular dark field (HAADF) detector, followed by sequential collection of diffraction patterns using a camera detector at the bottom. By using virtual selected and objective apertures to isolate signals across multiple probe positions and diffraction peaks, individual Bragg peaks in reciprocal space were identified and correlated with real-space imaging to construct a composite image of the grain morphology (see figure 2). The analysis of this image allowed us to calculate an average grain size of the CuPc thin film in our control sample of  $42 \pm 0.7$  nm. This is comparable to the grain size reported for FePc deposited at room temperature, which can be tuned by adjusting the temperature of the substrate during deposition [18].

The TEM control sample was fabricated simultaneously with the BLG/h-BN device, sharing the same deposition conditions. We can therefore assume a similar CuPc grain distribution in the CuPc/BLG/h-BN transport device. Understanding the molecular arrangement of the molecules on BLG/h-BN is important, as the size of the crystalline domains can potentially influence the charge transfer and addition of scatterers to the original device, as will be developed later.

## 4. Electronic transport measurements at low temperatures

We characterized our BLG/h-BN transport device through electronic transport measurements at low temperatures before the deposition of the CuPc molecules. Experiments were performed in a closed cycle cryostat with a superconducting magnet, where the differential resistance  $dV/dI$  in a two-probe setup was measured by modulating a bias current of typical amplitude 10–100 nA and measuring the voltage drop through standard lock-in detection. A measurement of the backgate voltage dependence of the resistance showed that our device was initially electron doped. Upon deposition of the CuPc molecules, we observed an important shift of the Dirac point, of about 48 V towards the positive voltages, indicating the hole doping of the BLG/h-BN device and a transfer of electrons from the BLG/h-BN to CuPc of  $(3.6 \pm 0.05) \times 10^{12} \text{ cm}^{-2}$  (see figure 3). The uncertainty on the charge transfer was calculated from the error of the fits presented in the supplemental material [14], that allow to determine the gate voltage value of the charge neutrality point  $V_D$ . The uncertainty for  $V_D$ ,  $\Delta V_D = \pm 0.7$  V affects all quantities that depend on the gate voltage or the electronic density, presented in this section. The value found for  $\Delta V_D$  coincides with the gate voltage step used for the back gate-dependent resistance measurements.



The previously mentioned electron transfer from graphene to CuPc is equivalent to the transfer of  $67 \pm 1$  electrons from BLG/h-BN to each CuPc grain. This is translated in a Fermi energy shift of  $120 \pm 2$  meV in the BLG, calculated using the relation between the Fermi energy and the Fermi wave vector, that for BLG is  $E = \frac{\hbar^2 k_F^2}{2m^*}$ , with  $k_F = \sqrt{n\pi}$ . This important charge transfer can be understood through the work function values of the materials involved. Graphene's work function on  $\text{SiO}_2$  is known to be  $4.6$  eV, being slightly larger for BLG ( $\approx 4.7$  eV) [19]. Recent works that use Kelvin probe force microscopy have found a work function of  $4.6$  eV for quasi-free standing BLG [20], that represents a closer situation to a BLG/h-BN heterostructure, where the BLG is isolated from the  $\text{SiO}_2$  charge impurities. For CuPc in the form of a thin film, scanning electron microscopy experiments

report a work function of  $\approx 4.9$  eV [21]. These values explain CuPc acting as an electron acceptor in our CuPc/BLG/h-BN device. Similarly to CuPc, FePc has been reported to be an electron acceptor when in contact to graphene [22], while vanadyl-Pc on graphene acts as an electron donor [23].

Surprisingly, the deposition of the CuPc thin film on the BLG/h-BN device creates only a small degradation of the mobility and mean free path of the original device, demonstrating that the CuPc thin film has a minimal effect on the landscape of long and short range scatterers that limit the mobility in graphene. This is in contrast to adatoms, that while able to offer new functionalities to graphene, are highly detrimental to its mobility [5, 6, 24–26]. We use the Drude formula to calculate the mobility of our device  $\mu = \frac{\sigma}{en}$  and the capacitor model to estimate the electronic density at different gate voltages,  $n = \frac{\epsilon_0 \epsilon_r}{ed} (V_g - V_D)$ , with  $V_D$  the gate voltage of the Dirac point (see supplemental material [14]). We deduce an electron mobility for our BLG/h-BN device of  $3200 \pm 200 \text{ cm}^2 \text{ Vs}^{-1}$  away from the Dirac point (at  $-1 \times 10^{12} \text{ cm}^{-2}$  carrier density) before the deposition of CuPc, becoming  $2800 \pm 100 \text{ cm}^2 \text{ Vs}^{-1}$  after the deposition of the molecules. This small degradation of the mobility suggests that CuPc might be neutralizing charged impurities in the original BLG/h-BN device. We also calculated the mean free path at the electron density  $1 \times 10^{12} \text{ cm}^{-2}$  from the diffusion coefficient  $D \equiv v_F l_{tr} / 2$ , where  $v_F = \hbar k_F / m^*$  for BLG. The diffusion coefficient is related to the conductivity through Einstein's relation  $D = \frac{\sigma}{e^2 \rho(E_F)}$  [27]. Using the density of states at the Fermi level for BLG  $\rho(E_F) = \frac{2m^*}{\pi \hbar^2}$  yields  $l_{tr} = \frac{\hbar \sigma}{2k_F e^2}$ , an expression that is in fact independent on the dispersion relation of the two-dimensional system [28]. We find an electron mean free path  $l_{tr}$  for electrons away from the Dirac point of  $37 \pm 1$  nm, that becomes  $32 \pm 1$  nm after the deposition of the molecules (see figure S5

in supplemental material [14]). Calculating the mean free path allows us to estimate  $k_{\text{F}}l_{\text{tr}}$ , which measures the effect of disorder on electronic wave functions.  $k_{\text{F}}l_{\text{tr}} \gg 1$  corresponds to a weakly disordered system and a good conductor, while  $k_{\text{F}}l_{\text{tr}} \ll 1$  is characteristic of an insulator with strongly localized electronic wave functions [28]. This value changes from  $6.7 \pm 0.3$  for the BLG/h-BN device to  $5.7 \pm 0.2$  after the deposition of CuPc, measured at  $1 \times 10^{12} \text{ cm}^{-2}$  electron carrier density. The small change in the value of  $k_{\text{F}}l_{\text{tr}}$  shows that the addition of the molecules has no major impact on the disorder of the device. As previously mentioned, the conductivity can be expressed in terms of  $k_{\text{F}}l_{\text{tr}}$  ( $\sigma = (2e^2/h)l_{\text{tr}}k_{\text{F}}$ ). The change in  $k_{\text{F}}l_{\text{tr}}$  can also be deduced when inspecting the conductivity in units of  $2e^2/h$  (see figure S4 in supplemental material [14]).

By plotting the conductivity, we can also quantify the increase of the width of the Dirac point, from  $8.6 \pm 0.4 \text{ V}$  in the BLG/h-BN device to  $10 \pm 0.4 \text{ V}$  after the deposition of the CuPc molecules (see figure S4 from the supplemental material [14]). This corresponds to a change from  $(0.65 \pm 0.05) \times 10^{12} \text{ cm}^{-2}$  to  $(0.76 \pm 0.05) \times 10^{12} \text{ cm}^{-2}$ . Such result can be understood within the approach of Adam, Das Sarma *et al* [29] as an increase of the residual electronic density. In their approach, the main scattering mechanism at low carrier densities comes from charged long-range impurities that create a non-uniform electron-hole puddle landscape [30], understood as the main cause of a minimum conductivity plateau in graphene [31]. Within this frame, CuPc molecules add some few charge impurities to the original BLG/h-BN device,  $(0.11 \pm 0.05) \times 10^{12} \text{ cm}^{-2}$ , corresponding to  $2 \pm 1$  charged impurities per CuPc grain.

We can also estimate the transport time  $\tau_{\text{tr}} = l_{\text{tr}}/v_{\text{F}}$ , the momentum relaxation time, given by an individual collision that destroys the initial momentum of the electrons [27]. We find  $\tau_{\text{tr}} = (6.0 \pm 0.2) \times 10^{-14} \text{ s}$ , coincidentally, very close to the value measured in the past at the same electron density ( $1 \times 10^{12} \text{ cm}^{-2}$ ) for a BLG through magnetoresistance measurements [32, 33]. The deposition of the molecules change this time to  $\tau_{\text{tr}} = (5.2 \pm 0.2) \times 10^{-14} \text{ s}$ . (See figure S5 from the supplementary materials).

The preserved mobility and mean free path after the deposition of CuPc is consistent with previous reports on other molecules in graphene, such as C<sub>60</sub> [34] and Pt-porphyrines [4]. The latter are similar to the phthalocyanines, with a macrocyclic structure with delocalized  $\pi$  electrons, similar to CuPc. Pt-porphyrins have been reported not only to preserve, but in some cases to improve the mobility of graphene upon the deposition of the molecules [4]. Similar results have been found with other planar molecules on graphene [35]. It is worth pointing out that in the works with planar molecules, the molecules are dispersed in a solution and drop casted

on the graphene device, and in some cases annealed to remove the solvent [35], a process that can unintentionally improve the mobility of the original device. Additionally, the crystallinity of the deposited molecules is unknown. This is in contrast to the CuPc molecules in the present work, that are deposited through a low temperature thermal evaporation while the BLG/h-BN remains at room temperature, and where a control TEM-compatible device gives information about the arrangement of the molecules on the device.

We now turn to the analysis of the weak localization in the BLG/h-BN before and after the deposition of the CuPc thin film. In BLG, the quantum correction to the Drude conductivity, as a function of magnetic field is given by [2]:

$$\Delta\sigma(B) = \frac{e^2}{\pi h} \left[ F\left(\frac{B}{B_{\phi}}\right) - F\left(\frac{B}{B_{\phi} + 2B_i}\right) + 2F\left(\frac{B}{B_{\phi} + B_*}\right) \right],$$

$$F(z) = \ln z + \psi\left(\frac{1}{2} + \frac{1}{z}\right), \quad B_{\phi,i,*} = \frac{\hbar}{4De} \tau_{\phi,i,*}^{-1}, \quad (1)$$

where the characteristic fields  $B_{\phi,i,*}$  are expressed in terms of various characteristic scattering times.  $B_{\phi}$  is related to the phase coherence time  $\tau_{\phi}^{-1}$ ,  $B_i$  is related to the intervalley scattering time  $\tau_i^{-1}$ , and  $B_*$  to a combined scattering time  $\tau_*^{-1}$ , with

$$\tau_*^{-1} = \tau_i^{-1} + \tau_w^{-1},$$

where  $\tau_w$  is the intravalley warping time combined with the time of chirality breaking [2].  $\psi$  is the digamma function. Other theoretical works have included the contribution of other intravalley scattering rates, such as  $\tau_z$ , associated to certain Cooperon modes, particle-particle correlation functions that determine the interference correction to the conductivity [3].

Magnetoconductance measurements were performed in a small field range ( $-0.3 \text{ T}$  to  $0.3 \text{ T}$ ) before and after CuPc deposition as shown in figure 4. Measurements were carried out at two different temperatures, 1.5 K and 5 K to corroborate the decrease of the quantum interference effects with the increasing temperature. The data collected was then fitted to equation (1) to extract the three scattering times ( $\tau_{\phi}^{-1}, \tau_i^{-1}, \tau_w^{-1}$ ) at these temperatures, represented in figure 4. We can see that  $\tau_{\phi}$  decreases with temperature as expected. It is also noticeable that the addition of CuPc has an impact on all the characteristic times. It decreases the phase coherence time  $\tau_{\phi}$ , that quantifies the typical travel time of an electronic wave packet before losing its phase coherence. From the behavior of  $\tau_{\phi}$ , we can infer the coupling of the interfering electrons to the environment, composed in general

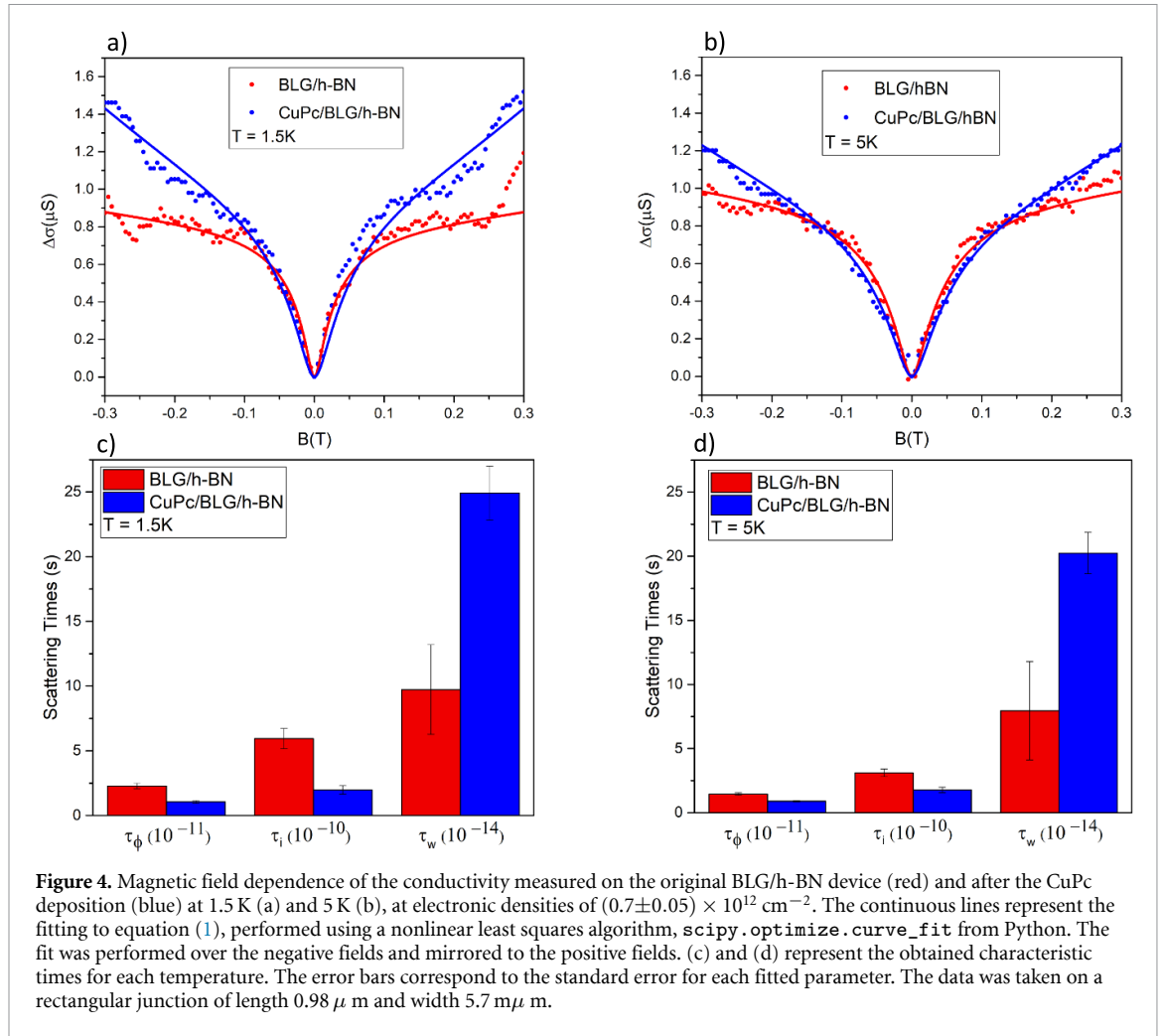


**Figure 4.** Magnetic field dependence of the conductivity measured on the original BLG/h-BN device (red) and after the CuPc deposition (blue) at 1.5 K (a) and 5 K (b), at electronic densities of  $(0.7 \pm 0.05) \times 10^{12} \text{ cm}^{-2}$ . The continuous lines represent the fitting to equation (1), performed using a nonlinear least squares algorithm, `scipy.optimize.curve_fit` from Python. The fit was performed over the negative fields and mirrored to the positive fields. (c) and (d) represent the obtained characteristic times for each temperature. The error bars correspond to the standard error for each fitted parameter. The data was taken on a rectangular junction of length  $0.98 \mu\text{m}$  and width  $5.7 \text{ m}\mu\text{m}$ .

by other electrons, phonons, electromagnetic fluctuations, magnetic impurities, etc. Oftentimes,  $\tau_\phi$  is related to inelastic collisions, however in some cases, phase breaking processes do not involve an exchange of energy between the interfering electron and its environment, leading to a temperature independent value. This is the case for example of scattering with paramagnetic impurities that create a spin flipping of the interfering electron [36]. In our case, both the deposition of CuPc and the temperature of the device have an impact on  $\tau_\phi$ , showing that the phase breaking occurs in scattering events that go beyond energy-conservation processes such as spin-flip scattering with the paramagnetic CuPc molecules. The phase coherent time in the original BLG/h-BN device,  $\tau_\phi = (2.3 \pm 0.2) \times 10^{-11} \text{ s}$  dropped by a factor of 2 after the deposition of the molecules,  $\tau_\phi = (1.1 \pm 0.1) \times 10^{-11} \text{ s}$ , remaining 3 orders of magnitude larger than  $\tau_e$ . We deduce therefore that the motion of the electrons over a phase relaxation time is not ballistic. In this regime, the length of the electronic trajectories over the time period  $\tau_\phi$  can be understood as the sum of short trajectories in random directions, given by  $l_\phi = \sqrt{D\tau_\phi}$  [27], known as the phase coherent length, that in our sample changes from  $460 \pm 30 \text{ nm}$

to  $290 \pm 20 \text{ nm}$  after the deposition of the molecules. It is interesting to note that the electronic trajectories keep their phase coherence even when scattered across different CuPc grains, that have an average size of  $42 \pm 0.7 \text{ nm}$ .

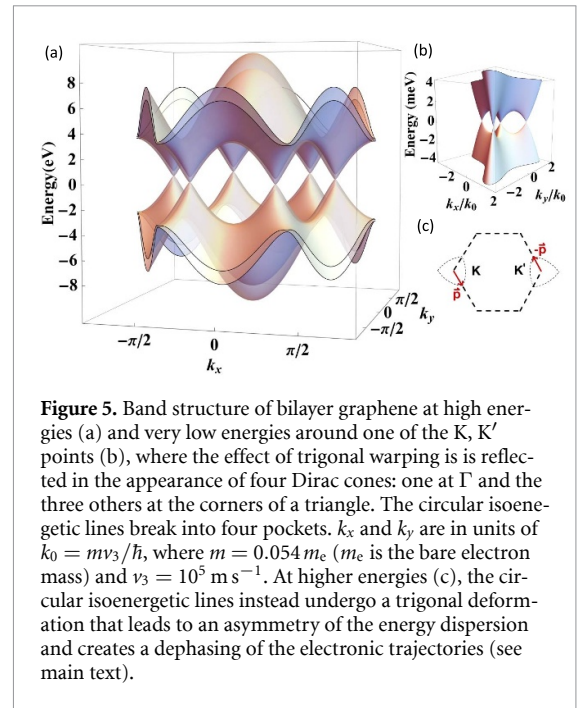
Given that the size of our sample is larger than the phase coherent length ( $L = 980 \text{ nm}$ ,  $W = 5.7 \mu\text{m}$  vs  $l_\phi = 460 \pm 30 \text{ nm}$ ), the amplitude of the universal conductance fluctuations is small and did not interfere with the observation of weak localization.

From our fit to the theory of weak localization for BLG, we also deduce the intervalley scattering time  $\tau_i$ , the time it takes for carriers to scatter from one valley to the other. We find a value of the order of  $10^{-10} \text{ s}$ , about 1 order of magnitude larger than the values reported in the past for BLG on  $\text{SiO}_2$  [2]. The larger values reported here can be consequence of the h-BN isolating the BLG from scatterers from the substrate and therefore disfavoring intervalley scattering. We find that  $\tau_i$  decreases after the deposition of the molecules, from  $\tau_i = (5.9 \pm 0.78)$  to  $(2.0 \pm 0.33) \times 10^{-10} \text{ s}$ . In general, intervalley scattering requires sharp defects, such at the edges of the sample, as it takes a large momentum transfer to change electrons from one valley to the other [1].

The observed reduction of  $\tau_i$  after the CuPc deposition, indicates an increase in scattering between the K and K' valleys due to the presence of the molecules. We can estimate the intervalley diffusion length,  $L_i = \sqrt{D\tau_i}$ , that measures a characteristic distance between defects that can significantly change the momentum of the carriers [2]. This characteristic length changes from  $L_i = 2.3 \pm 0.2 \mu\text{m}$  to  $1.3 \pm 0.1 \mu\text{m}$  after CuPc, indicating that carriers remain in the same valley through collisions that extend over multiple grains of CuPc.

Finally, our fit to the magnetoresistance provides information about a very interesting elastic process that is strong in BLG compared to its monolayer counterpart, the warping on the energy spectrum, characterized by  $\tau_w$  [3]. By fitting our data to the model of Gorbachev *et al* [2] that considers  $\tau_*$  dependent only on  $\tau_i$  and  $\tau_w$ , and using a non-linear least squares fitting algorithm, we extract all characteristic times. As a first approach, we fit our data to equation (1), extracting  $\tau_\phi$ ,  $\tau_i$  and  $\tau_*$ , and considering no dependence of  $\tau_*$  on the other characteristic times. The results are summarized in table I in the supplemental material [14]. There is a clear increase in the intravalley scattering time  $\tau_*$  upon the deposition of the CuPc molecules. We performed next a more elaborated fit to equation (1) considering that  $\tau_*^{-1} = \tau_i^{-1} + \tau_w^{-1}$ . The values found for  $\tau_w$  in the second fit are almost identical to those found in the first fit for  $\tau_*$  (to the first 2 significant figures), as seen in table II in the supplemental material [14]. This is expected, given that  $\tau_i$  is larger than  $\tau_*$  by three orders of magnitude, making that in the second fit, the behavior of  $\tau_w$  is very similar, if not identical, to the one of  $\tau_*$ .

As mentioned before,  $\tau_w$  is related to trigonal warping, a three-fold perturbation of the circular isoenergetic lines that are characteristic of BLG (as well as monolayer graphene) near each K and K' valley (see figure 5). It occurs at high energies, as the band structure mimics the symmetry of the crystal lattice, where the consideration of nearest-neighbor hopping leads to a complex momentum dependence [37]. In BLG and bulk graphite, trigonal warping also appears at low energies as a result of the skew interlayer hopping between carbon atoms that do not lie directly above or below each other and are therefore not coupled through strong interlayer hopping. Such oblique coupling is quantified by the tight-binding parameter  $\gamma_3$ , and has an important influence on the band structure at very low energies. At a threshold energy of  $\approx 1$  meV, the isoenergetic lines go through a Lifshitz transition, breaking into four pockets, corresponding to four Dirac cones, one at  $\Gamma$  and three others at the corners of a triangle [37]. Above this energy, the effect of the  $\gamma_3$  coupling can be treated as a perturbation, and creates a trigonal deformation of the circular single-connected Fermi line leading to an asymmetry of the energy dispersion:



$\epsilon(\mathbf{K}, \mathbf{p}) \neq \epsilon(\mathbf{K}, -\mathbf{p})$ , with  $\epsilon(\mathbf{K}, \mathbf{p}) = \epsilon(\mathbf{K}', -\mathbf{p})$  and  $\mathbf{p}$  measured with respect to the center of the valley [3] (see figure 5(c)). Such deformation of the Fermi line has been experimentally observed through quasiparticle scattering experiments that show a triangular shape of the Fermi surface near K and K' at energies up to 112 meV [38]. The  $\mathbf{p} \rightarrow -\mathbf{p}$  asymmetry of the dispersion at each K and K' valley, creates a dephasing of electronic trajectories as those discussed at the introduction, and is characterized by the characteristic time  $\tau_w$  [12]. Trigonal warping can therefore potentially destroy the manifestation of chirality in the localization properties of BLG, leading to the suppression of weak localization [3, 12]. When there is a strong scattering due to trigonal warping ( $\tau_w \rightarrow 0$ ) and no intervalley scattering ( $\tau_i \rightarrow \infty$ ), the third term in equation (1) disappears while the first two cancel each other, resulting in a zero magnetoconductance and a complete vanishing of weak localization. If instead there is some intervalley scattering, the second term in equation (1) is smaller than the first term, and there is some weak localization. This is the case in our experiment as well as in previous reports [2]. In our work, we find that the intervalley scattering time  $\tau_i$  is 10 times larger than the phase coherent time  $\tau_\phi$ . Also, the intervalley diffusion length  $L_i$  is about 2 times larger than the length of the measured junction ( $1 \mu\text{m}$ ). We still find, however, a weak localization correction at zero fields (see figure 4(a)), indicating that there are some intervalley scattering events across the measured junction.

Figure 4(a) shows that the addition of the CuPc molecules enlarges the weak localization correction in our graphene/h-BN sample, reflected in a  $\tau_*$  (or a  $\tau_w$ ) that is 2.5 times larger than the one measured in the original BLG/h-BN device,  $(25 \pm 2) \times$

$10^{-14}$  vs  $(9.7 \pm 4) \times 10^{-14}$  s. These values correspond to energies of 26–68 meV, which coincides with the energy scale where trigonal warping effects are important in BLG. The increase in  $\tau_w$  suggests that the addition of the molecules has a tendency to bring back the manifestation of the carrier chirality in the localization of BLG, by reducing trigonal warping-related scattering events. Figure S7 of the supplementary materials shows a fit to the magnetoresistance data after the deposition of CuPc using the  $\tau_w$  found before the deposition of the molecules, which puts in evidence the validity of the fit for  $\tau_w$  after the deposition of the molecules.

## 5. Conclusion

We have characterized a heterostructure of CuPc/BLG/h-BN, where the crystallinity of the CuPc thin film on the BLG/h-BN was identified through the analysis of a TEM-compatible control sample, studied through 4D-STEM, a diffraction space imaging technique that minimizes the radiation damage of the CuPc molecules. This technique provided an estimate of the size of the crystalline grains of CuPc on our transport sample, of about  $\approx 42$  nm. Electronic transport measurements at low temperatures before and after the deposition of the molecules revealed an important charge transfer of electrons from the BLG/h-BN to the CuPc molecules, of  $3.6 \times 10^{12} \text{ cm}^{-2}$  corresponding to  $\approx 67$  electrons transferred to each grain of CuPc. Unexpectedly, we found a preservation of the mobility of the BLG/h-BN device upon the deposition of the molecules, degraded only by 13%. The width of the Dirac point lightly increased, that we interpreted as the CuPc adding some few charged impurities to the device, about  $\approx 2$  impurities per grain of CuPc. Most importantly, our weak localization measurements disclosed that while the deposition of the molecules creates more scattering events that break the phase coherence of the carriers and that transfer electrons from one valley to the other, surprisingly, it triggers an improvement of trigonal warping time  $\tau_w$ . This corresponds to a reduction of the scattering associated to the trigonal deformation of BLG's Fermi surface near K and K'. As trigonal warping is known to destroy weak localization effects, our results suggest that the deposition of the CuPc molecules has tendency to restore weak localization in BLG and therefore the manifestation of the chirality of the carriers in this system. The effect of these large molecules on the electronic structure of BLG is not completely unexpected. CuPc in its  $\alpha$  phase crystallizes into space group C2/c with  $a = 25.92 \text{ \AA}$ ,  $b = 3.79 \text{ \AA}$  and  $c = 23.92 \text{ \AA}$  [39]. In a lying down configuration, this corresponds to  $k = 0.24\text{--}0.26 \text{ \AA}^{-1}$ , similar to the momentum range in which trigonal warping has been experimentally observed around the K and K' valleys in BLG [38]. Further

experiments with phthalocyanines with no magnetic moment such as the metal-free Pc H<sub>2</sub>Pc or those capable of developing long range ferromagnetism such as MnPc and FePc, can bring light on the effect of the magnetic moment on this phenomenon of restoration of weak localization in BLG.

## Data availability statement

The data cannot be made publicly available upon publication because they are not available in a format that is sufficiently accessible or reusable by other researchers. The data that support the findings of this study are available upon reasonable request from the authors.

Supplementary Materials available at <https://doi.org/10.1088/2053-1583/ae4367/data1>.

## Acknowledgments

The primary funding for this work was provided by the U.S. Department of Energy, Office of Science, Office of Basic Energy Sciences under contract DE-SC0018154 for electronic transport measurements, data analysis, sample fabrication and Raman characterization. The deposition of the molecular thin film was funded by the Cal. State. Long Beach and the Ohio State University Partnership for Education and Research in Topological Materials, a National Science Foundation PREM, under Grant No. 2425133. 4D-STEM measurements were possible thanks to BioPACIFIC MIP, an NSF Materials Innovation Platform (DMR-1933487). Preliminary TEM measurements by Y C, H C and B C R were funded by the National Science Foundation, DMR-1548924 (STROBE). K W and T T acknowledge support from the JSPS KAKENHI (Grant Numbers 21H05233 and 23H02052), the CREST (JPMJCR24A5), JST and World Premier International Research Center Initiative (WPI), MEXT, Japan for the h-BN growth. We would like to acknowledge very insightful discussions with Francisco Guinea, Maria Jose Calderon, Andreas Bill, Sophie Guéron and Hélène Bouchiat as well as invaluable advice from David Warren from Oxford Instruments. D D, M M and E C-O would like to acknowledge the Google American Physical Society Bridge Program, M K D D M the Google summer assistantship at CSULB. A M would like to acknowledge the Keung Luke, Charles Roberts and Richard Whiteley Endowed Scholarship at CSULB.

## ORCID iDs

Anise Mansour  0000-0001-5718-6721

Kenji Watanabe  0000-0003-3701-8119

Thomas Gredig  0000-0002-5824-7626

Claudia Ojeda-Aristizabal  0000-0003-0816-9727

## References

- [1] Tikhonenko F V, Kozikov A A, Savchenko A K and Gorbachev R V 2009 Transition between electron localization and antilocalization in graphene *Phys. Rev. Lett.* **103** 226801
- [2] Gorbachev R V, Tikhonenko F V, Mayorov A S, Horsell D W and Savchenko A K 2007 Weak localization in bilayer graphene *Phys. Rev. Lett.* **98** 176805
- [3] Kechedzhi K, Fal'ko V I, McCann E and Altshuler B L 2007 Influence of trigonal warping on interference effects in bilayer graphene *Phys. Rev. Lett.* **98** 176806
- [4] Li C, Komatsu K, Bertrand S, Clavé G, Campidelli S, Filoramo A, Guéron S and Bouchiat H 2016 Signature of gate-tunable magnetism in graphene grafted with pt-porphyrins *Phys. Rev. B* **93** 045403
- [5] Chandni U, Henriksen E A and Eisenstein J P 2015 Transport in indium-decorated graphene *Phys. Rev. B* **91** 245402
- [6] Elias J A and Henriksen E A 2017 Electronic transport and scattering times in tungsten-decorated graphene *Phys. Rev. B* **95** 075405
- [7] Bartolome J, Monton C and Schuller I K 2014 Magnetism of metal phthalocyanines *Molecular Magnets: Physics and Applications* ed J Bartolome, F Luis and J F Fernandez (Springer) pp 221–45
- [8] Afzal A M, Khan M F, Nazir G, Dastgeer G, Aftab S, Akhtar I, Seo Y and Eom J 2018 Gate modulation of the spin-orbit interaction in bilayer graphene encapsulated by WS<sub>2</sub> films *Sci. Rep.* **8** 3412
- [9] Icking E, Wörtche F, Cummings A W, Wörtche A, Watanabe K, Taniguchi T, Volk C, Beschoten B and Stampfer C 2025 Weak localization as probe of spin-orbit-induced spin-split bands in bilayer graphene proximity coupled to WSe<sub>2</sub> (arXiv:2505.24632 [cond-mat.mes-hall])
- [10] Le D, Barinov A, Preciado E, Isarraraz M, Tanabe I, Komesu T, Troha C, Bartels L, Rahman T S and Dowben P A 2015 Spin-orbit coupling in the band structure of monolayer wse<sub>2</sub> *J. Phys.: Condens. Matter* **27** 182201
- [11] Stepanow S, Mugarza A, Ceballos G, Moras P, Cezar J C, Carbone C and Gambardella P 2010 Giant spin and orbital moment anisotropies of a cu-phthalocyanine monolayer *Phys. Rev. B* **82** 014405
- [12] Kechedzhi K, McCann E, Fal'ko V I, Suzuura H, Ando T and Altshuler B L 2007 Weak localization in monolayer and bilayer graphene *Eur. Phys. J. Spec. Top.* **148** 39–54
- [13] Zomer P J, Dash S P, Tombros N and van Wees B J 2011 A transfer technique for high mobility graphene devices on commercially available hexagonal boron nitride *Appl. Phys. Lett.* **99** 232104
- [14] See Supplemental Material at <https://doi.org/10.1088/2053-1583/ae4367>, for details on the sample fabrication, the Raman scan of the CuPc/BLG/h-BN device, tables of the scattering times extracted from the fittings of the WL data, details on the analysis of the 4D-STEM data for the extraction of the size of the crystalline grains of CuPc, fits to the conductivity of the device that allow us to deduce the value of the Dirac point and its uncertainty, as well as the back gate dependence of the mobility and mean free path in the device before and after the deposition of CuPc. The Supplemental material also contains references [11, 12].
- [15] Fates R, Bouridah H and Raskin J-P 2019 Probing carrier concentration in gated single, bi- and tri-layer cvd graphene using raman spectroscopy *Carbon* **149** 390–9
- [16] Ling X, Fang W, Lee Y-H, Araujo P T, Zhang X, Rodriguez-Nieva J F, Lin Y, Zhang J, Kong J and Dresselhaus M S 2014 Raman enhancement effect on two-dimensional layered materials: Graphene, h-bn and mos<sub>2</sub> *Nano Lett.* **14** 3033–40
- [17] Zou K, Hong X and Zhu J 2011 Effective mass of electrons and holes in bilayer graphene: electron-hole asymmetry and electron-electron interaction *Phys. Rev. B* **84** 085408
- [18] Gentry K P, Gredig T and Schuller I K 2009 Asymmetric grain distribution in phthalocyanine thin films *Phys. Rev. B* **80** 174118
- [19] Yu Y-J, Zhao Y, Ryu S, Brus L E, Kim K S and Kim P 2009 Tuning the graphene work function by electric field effect *Nano Lett.* **9** 3430–4
- [20] Melios C, Panchal V, Giusca C E, Strupinski W, Silva S R P and Kazakova O 2015 Carrier type inversion in quasi-free standing graphene: studies of local electronic and structural properties *Sci. Rep.* **5** 10505
- [21] Vijayan L, Thomas A, Kumar K S and Jinesh K 2018 Low power organic field effect transistors with copper phthalocyanine as active layer *J. Sci. Adv. Mater. Dev.* **3** 348–52
- [22] Pan H, Wang X, Wang Q, Wu X, Liu C, Lin N and Zhao Y 2021 Proximity effect of epitaxial iron phthalocyanine molecules on high-quality graphene devices *Chin. Phys. Lett.* **38** 087201
- [23] Wang X, Xu J-B, Xie W and Du J 2011 Quantitative analysis of graphene doping by organic molecular charge transfer *J. Phys. Chem. C* **115** 7596–602
- [24] Hong X, Cheng S-H, Herding C and Zhu J 2011 Colossal negative magnetoresistance in dilute fluorinated graphene *Phys. Rev. B* **83** 085410
- [25] Withers F, Dubois M and Savchenko A K 2010 Electron properties of fluorinated single-layer graphene transistors *Phys. Rev. B* **82** 073403
- [26] Alemani M, Barfuss A, Geng B, Girit C, Reisenauer P, Crommie M F, Wang F, Zettl A and Hellman F 2012 Effect of gadolinium adatoms on the transport properties of graphene *Phys. Rev. B* **86** 075433
- [27] Datta S 1995 *Electronic Transport in Mesoscopic Systems* (Cambridge University Press) p 16–17, 39–41, 21–22
- [28] Akkermans E and Montambaux G 2004 *Physique mésoscopique des électrons et des Photons* pp 293–4
- [29] Adam S, Hwang E H, Galitski V M and Das Sarma S 2007 A self-consistent theory for graphene transport *Proc. Natl Acad. Sci. USA* **104** 18392–7
- [30] Zhang Y, Brar V W, Girit C, Zettl A and Crommie M F 2009 Origin of spatial charge inhomogeneity in graphene *Nat. Phys.* **5** 722–6
- [31] Chen J-H, Jang C, Adam S, Fuhrer M S, Williams E D and Ishigami M 2008 Charged-impurity scattering in graphene *Nat. Phys.* **4** 377–81
- [32] Monteverde M, Ojeda-Aristizabal C, Weil R, Bennaceur K, Ferrier M, Guéron S, Glatli C, Bouchiat H, Fuchs J N and Maslov D L 2010 Transport and elastic scattering times as probes of the nature of impurity scattering in single-layer and bilayer graphene *Phys. Rev. Lett.* **104** 126801
- [33] Monteverde M, Ojeda-Aristizabal C, Komatsu K, Li C, Ferrier M, Guéron S and Bouchiat H 2012 What are the relevant disorder scales for quantum transport in graphene? *J. Low Temp. Phys.* **167** 1–14
- [34] Ojeda-Aristizabal C *et al* 2017 Molecular arrangement and charge transfer in c60/graphene heterostructures *ACS Nano* **11** 4686–93
- [35] Datta S, Cai Y, Yudhistira I, Zeng Z, Zhang Y-W, Zhang H, Adam S, Wu J and Loh K P 2017 Tuning magnetoresistance in molybdenum disulphide and graphene using a molecular spin transition *Nat. Commun.* **8** 677
- [36] Akkermans E, Montambaux G, Pichard J-L and Zinn-Justin J (eds) 1996 *Les Houches, Session LXI, 28 Juin - 29 Juillet 1994 : Physique Quantique méSoscopique = Mesoscopic Quantum Physics, (Les Houches Summer School Proceedings)* (Elsevier Science)
- [37] McCann E and Koshino M 2013 The electronic properties of bilayer graphene *Rep. Prog. Phys.* **76** 056503
- [38] Joucken F, Ge Z, Quezada-López E A, Davenport J L, Watanabe K, Taniguchi T and Velasco J 2020 Determination of the trigonal warping orientation in bernal-stacked bilayer graphene via scanning tunneling microscopy *Phys. Rev. B* **101** 161103
- [39] Bartolome Sanjoaquin J, Fernando L and Fernandez J F 2016 *Molecular Magnets Physics and Applications*